CHAPTER 14

CO_2 photoconversion catalyzed by nanoparticles supported on TiO_2

Reyna Natividad
Chemical Engineering Laboratory, Joint Centre for Research on Sustainable Chemistry, Autonomous University of the State of Mexico, Toluca, Mexico

1. Introduction

For centuries, human beings have dedicated important intellectual and economical efforts into the generation of knowledge and development of technology, to increase quality of life. Although this has been achieved in many ways, all this development has also brought along a serious threat to global environmental sustainability and this is global warming. This phenomenon is mainly affected by greenhouse gases (GHG) such as carbon dioxide (CO_2), methane (CH_4), nitrous oxide (N_2O), and fluorinated compounds. Although the global warming potential (GWP) of methane and nitrous oxide is higher than that of CO_2, the last one represents more than 75% of the total emissions. Therefore, in the last decades, there has been an increasing concern worldwide about the capture and valorization of this gas through its conversion to fuels. To achieve so, some strategies can be distinguished: thermochemical, photochemical, electrochemical, photoelectrochemical, photothermochemical. This chapter is dedicated to a photocatalytic process, and therefore, this is further discussed.

The CO_2 photoconversion aims to produce value-added chemicals by means of catalyzing the CO_2 chemical reduction with a semiconductor activated by a light source, preferentially sun light, in order to increase the sustainability of the process. The assessed light sources vary in intensity and wavelength (254, 365, and 450 nm, mainly). The process can be conducted in two-phase or three-phase mode. In any of them, a reducing agent is required and the most assessed one has been water, either in vapor or liquid phase. The process is rather complex and the literature on this regard is nowadays vast because there are several factors affecting both, the yield and selectivity of the process. These factors being composition of the catalyst, catalyst

Nanoparticles in Green Organic Synthesis
https://doi.org/10.1016/B978-0-323-95921-6.00013-5

synthesis, reducing agent, type of reactor, light source, and macroscopic morphology of the catalyst (powders or films).

This chapter aims to present a review on the CO_2 photoconversion catalyzed by TiO_2-supported nanoparticles, copper and gold specifically, and some nanoalloys obtained with them. Fig. 1 summarizes the main products identified in such a process: CO, H_2, CH_4, CH_3OH, and multiple carbon compounds.

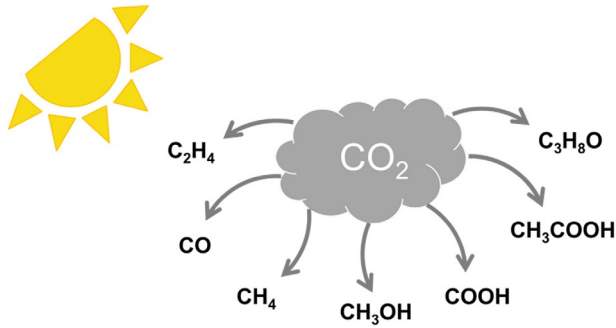

Fig. 1 Chemical compounds obtained from CO_2 photoconversion catalyzed by nanoparticles supported on TiO_2. *(Credit: Own elaboration.)*

The mixture CO and H_2 is well known as syngas or synthesis gas and can be directly used as fuel [1] or to produce hydrocarbons [2]. The conventional ways to produce syngas are by steam-methane reforming (reaction 1) and partial oxidation (reaction 2),

$$CH_4 + H_2O \xrightarrow{\text{catalyst}} CO + 3H_2 \tag{1}$$

$$CH_4 + \frac{1}{2}O_2 \rightarrow CO + 3H_2 \tag{2}$$

Reaction (1) is highly endothermic (206,000 kJ/kmol) while the second reaction is exothermic (−36,000 kJ/kmol) [2]. Anyway, syngas are desirable products since they can be turned into hydrocarbons by means of the general Fischer-Tropsch reaction (reaction 3),

$$2nH_2 + nCO \xrightarrow{\text{catalyst}} C_nH_{2n} + nH_2O \tag{3}$$

The produced hydrocarbons (C_nH_{2n}) by means of reaction (3) are determined by the catalyst, reaction temperature, and pressure [2].

Among the important compounds produced with syngas, there is methanol (CH_3OH)

$$CO + 2H_2 \rightarrow CH_3OH \quad (4)$$

Methanol production is of paramount importance as it is a versatile molecule that can be used as fuel (is the hydrocarbon with the highest hydrogen atoms to carbon atoms ratio). Compared to fossil fuels, the use of methanol as fuel reduces sulfide oxides emission by 99%, nitrogen oxides by 60%, and particulate matter by 95%. It can be used in fuel cells as hydrogen carrier and in the synthesis of various chemical compounds such as paints, plastics, carpeting, adhesives, sealants, lubricants, and many more [3].

In the context of CO_2 photoconversion, the production mechanisms and rates of the aforementioned compounds, when using copper and gold nanoparticles on TiO_2, will be revised in this chapter.

2. TiO_2-supported nanoparticles

TiO_2 is a semiconductor that exhibits a band gap of 3.2 eV and has been widely applied as a photocatalyst. This is due to its low operational temperature, its cost-effectiveness, abundance, nontoxicity, stability (strong resistance to chemicals and photocorrosion), and suitable electronic and optical properties [4,5]. Although the number of works related to the use of TiO_2 in the CO_2 photoconversion reaction has been increasing, such a number is not comparable with that where TiO_2 is used as a photocatalyst to conduct oxidation reactions.

The way TiO_2 acts as photocatalyst has been extensively documented and is depicted in Fig. 2. In summary, when a photon with enough energy hits the TiO_2 surface, an electron from the valence band (VB) is excited toward the conduction band (CB), generating a positively charged hole (h^+) in the former and an electron (e^-) in the latter; in such a way that water and some organic molecules are oxidized on the holes and then some molecules, like CO_2, are reduced with the available electrons at the CB. These reactions are constrained by the "life time" of the pair h^+-e^-, and therefore, this issue has become the subject of several investigations. Fig. 2 also shows the plausible products that could be obtained in the CO_2 photocatalytic reduction of carbon dioxide, catalyzed by TiO_2. These products being methane (CH_4), methanol (CH_3OH), hydrogen (H_2), and carbon monoxide (CO).

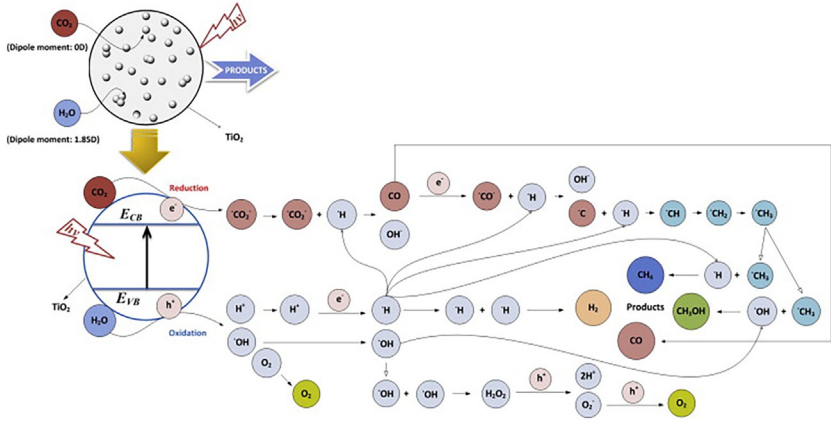

Fig. 2 Mechanism and pathways of the photocatalytic reduction of carbon dioxide with water vapor to fuels, catalyzed by bare TiO_2. *(Credit: Reprinted from P. Akhter, M. Hussain, G. Saracco, N. Russo, Novel nanostructured-TiO2 materials for the photocatalytic reduction of CO2 greenhouse gas to hydrocarbons and syngas, Fuel 149 (2015) 55–65, https://doi.org/10.1016/j.fuel.2014.09.079 with permission from Elsevier.)*

Fig. 3 summarizes some results obtained in the last years when conducting CO_2 photoreduction catalyzed by titania. The results depicted in Fig. 3 were extracted from Refs. [6–9]. The main identified products have been CO, H_2, and CH_4. The depicted results correspond to different investigations under different reaction conditions (radiation source and reducing agent), and therefore, a straightforward comparison is not plausible. Nevertheless, it is important to note the effect of the TiO_2 nanoarchitecture on the production rate of the aforementioned compounds. Interestingly, the use of TiO_2 nanoparticles or nanosheets seems to favor carbon monoxide production rate over methane and hydrogen [7]. TiO_2 nanosheets, under simulated solar radiation and water vapor, lead to the highest CO and CH_4 yields of approximately 30 and 13 μmol/g h, respectively [7]. As can be seen in Fig. 3, however, the yield is generally low and this has been ascribed mainly to a relatively rapid recombination of the generated pair h^+-e^-. Although not included in Fig. 3, nanotube arrays of TiO_2 have been presented [10] as a promising support of metallic particles, to produce not only CO and CH_4 but also multiple carbon compounds such as ethane (C_2H_6), ethylene (C_2H_4) and propene (C_3H_6).

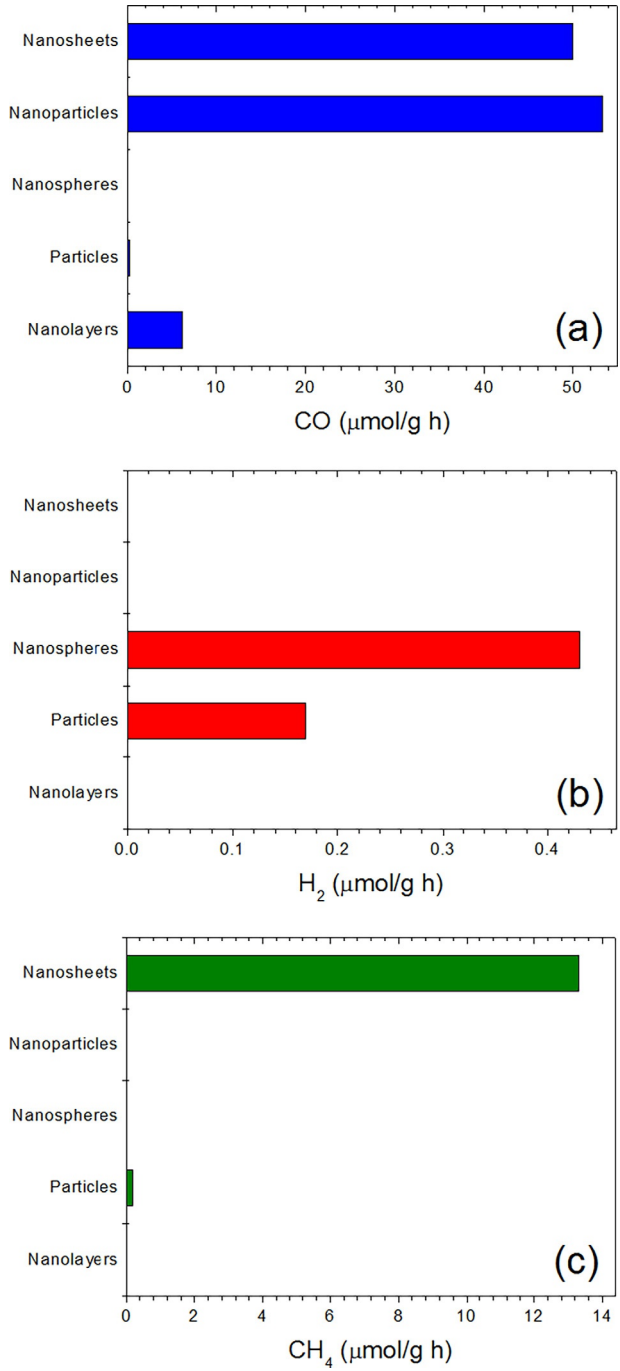

Fig. 3 Production rate of (A) carbon monoxide (CO), (B) hydrogen (H_2), and (C) methane (CH_4), during the CO_2 photoconversion catalyzed by bare TiO_2. *(Credit: Own elaboration.)*

A main strategy to improve the yield and selectivity of the CO_2 photoconversion toward certain molecules such as CH_4, CO, CH_3OH, CH_2O, and HCOOH has been to catalyze the reaction with catalytic systems constituted by metal nanoparticles or metallic nanoalloys supported on the TiO_2 surface. In this context, it can be seen in Fig. 4 the distribution of works dedicated to each metal. It is worth remembering that this analysis focuses only on nanoparticles.

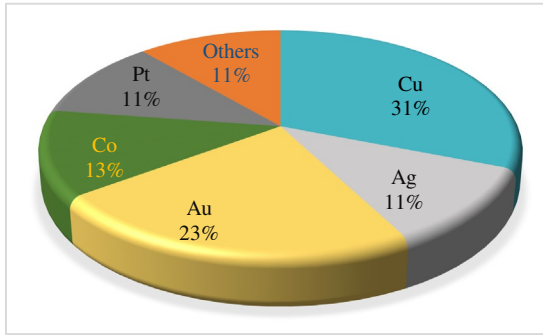

Fig. 4 Distribution of studies per metal nanoparticles supported on TiO_2. *(Credit: Own elaboration.)*

As shown in Fig. 4, the most studied metal is copper (Cu). This is because it decreases the recombination of the pair hole (h^+)-electron (e^-) generated in TiO_2, is an alkaline metal that favors CO_2 adsorption, transfers the electrons produced during the photo-activation of TiO_2, and is relatively low cost with high availability.

2.1 Copper nanoparticles and nanoalloys on TiO_2

CO_2 adsorption proceeds readily on alkaline materials and this is one of the reasons for the relatively large quantity of studies related to its photoreduction on Cu. Copper can be in metallic, cuprous (Cu^+), or cupric (Cu^{2+}) oxidation state. The reduction standard electrode potentials for copper are [6]

$$Cu^+ + e^- \leftrightarrow Cu^o \; E^0 = +0.159 \text{ eV} \tag{5}$$

$$Cu^{2+} + e^- \leftrightarrow Cu^+ \; E^0 = +0.520 \text{ eV} \tag{6}$$

$$Cu^{2+} + 2e^- \leftrightarrow Cu^o \; E^0 = +0.340 \text{ eV} \tag{7}$$

The oxidation state of copper has an effect on the h^+-e^- recombination process. The lower the oxidation state the higher is the restraining of the recombination process [4]. These are summarized in Table 1 the conducted

studies on the CO_2 photoreduction catalyzed by Cu nanoparticles and copper-based alloys supported on TiO_2 in the last decade. As can be seen in Table 1, the most used reaction medium is water. In this sense, two modes of carrying out the CO_2 photoreduction can be distinguished within literature, one with vapor and the other one with liquid water. This is relevant because the phase of water affects the product distribution on the surface of TiO_2 during CO_2 photoconversion [20–22]. Regarding product distribution, most works focus on the quantification of CO, H_2, and CH_4. Unfortunately, the production units are not homogenized, and this makes the comparison rather complex. Nevertheless, although a mixture of Cu^+/Cu^o is recommended to achieve the highest efficiency in the charges separation [11]; the results in Table 1 suggest decorating of TiO_2 with metallic copper as the most promising strategy in terms of CO and H_2 yield.

When the reaction is conducted in the gas phase, the reported mechanism on Cu^o/TiO_2 is summarized in Fig. 5 [4]. According to these authors, the first steps of the CO_2 photoreduction process catalyzed by Cu^o/TiO_2 are the adsorption of CO_2 at the Cu-TiO_2 interface and the generation of the pair hole (h^+)-electron (e^-), the former in the valence band and the latter on the conduction band of TiO_2, by means of light absorption. This migration is possible due to the Fermi level of the valence band being higher than that of Cu [23]. Then the copper transfers the generated e^- to the previously adsorbed CO_2 and CO is produced. An intermediate step in this process is the activation of the CO_2 molecule by the transferred e^-, thus generating the adsorbed radical-anion $CO_2^{\bullet -}$ which is converted in adsorbed HCO_2 ($^*HCO_2$) by the addition of a proton. These are believed to be the precursor species of CO, which is produced by the surface dissociation of $^*HCO_2$. Concomitantly, water is oxidized at the generated valence band holes (h^+). The dissociation of water may also proceed by the action of enough energetic light, like UV-C. It is important to note that according to the calculations conducted by [4], the CO desorption step demands higher energy than the others and then is favored by the use of UV-C light. If not enough energy is provided to the system to activate the CO desorption step, the catalyst will deactivate [4].

When the CO_2 photocatalytic reduction is conducted in liquid water and under UV-C light, the products distribution changes and C2 compounds appear (entry 4). Although this is also observed with the addition of Rh, at this point, the mechanism only with Cu will be discussed.

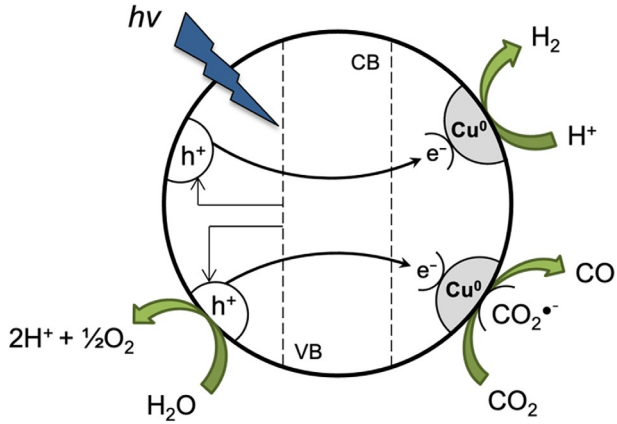

Fig. 5 Proposed mechanism by Ref. [4] of CO_2 photoreduction with water vapor, catalyzed by Cu^o/TiO_2. *(Credit: Own elaboration.)*

The mechanism of CO_2 photo-reduction catalyzed by Cu^o-TiO_2 in water includes the change in activation energy of CO_2 by reacting with water to produce carbonic acid. This occurs via reactions (8–11) [24,25], where the first step is the solution of CO_2 in water (reaction 8) and then this dissolved CO_2 reacts with water to produce carbonic acid (reaction 9) that is dissociated into anions, carbonate, and bicarbonate (reactions 10 and 11). This process is practically instantaneous and is enhanced when using alkaline solutions [25].

$$CO_{2\,(g)} \leftrightarrow CO_{2\,(aq)} \tag{8}$$

$$CO_{2\,(aq)} + H_2O_{(l)} \leftrightarrow H_2CO_{3\,(aq)} \tag{9}$$

$$H_2CO_{3\,(aq)} \leftrightarrow H^+_{(aq)} + HCO^{3-}_{(aq)} \tag{10}$$

$$HCO^{3-}_{(aq)} \leftrightarrow H^+_{(aq)} + CO_3{}^{2-}_{(aq)} \tag{11}$$

This carbonic acid is prone to be split by chemisorption onto Cu^+ and Cu^o, thus producing chemisorbed CO that is later dimerized to form the precursor of C2 compounds [24]. The production of single and multiple carbon compounds when using Cu/TiO_2 has been recently reported by [9]. According to the latter, the plausible set of reactions to produce hydrogen, carbon monoxide, methane, methanol, acetic acid, propanol, and acetone is depicted in Scheme 1.

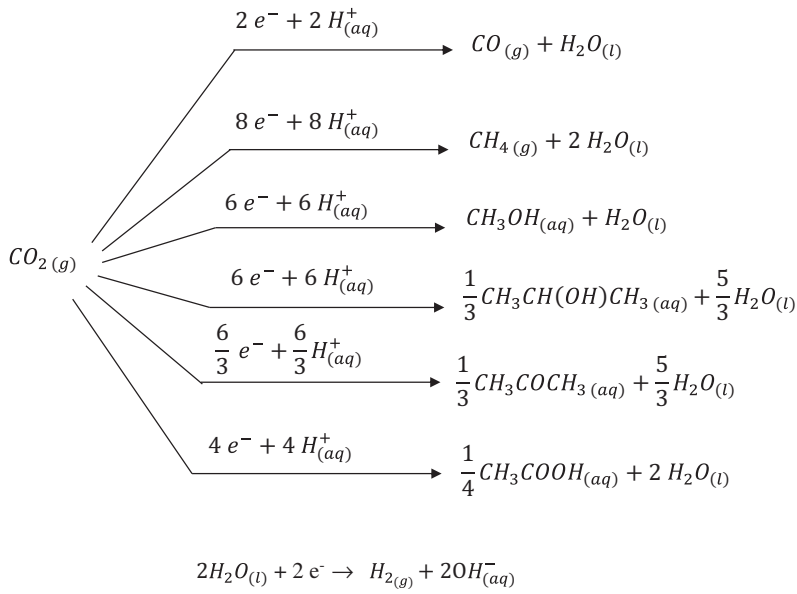

Scheme 1 Proposed reaction scheme to produce C1 and C2 compounds via CO_2 photoreduction with water (liquid) catalyzed by Cu^o/TiO_2.

Because of its competition for electrons, the suppression of last reaction in Scheme 1 is pursued. Water is also acknowledged to be oxidized in the valence band holes in TiO_2 as reported in other works [4,26]. Although this oxidation reaction does not consume electrons, it produces hydroxyl radicals that are able to oxidize the produced organic compounds, resulting in a yield decrease [18].

From reaction Scheme 1, it can be observed that the CO_2 photoreduction involves the transfer of proton-assisted multielectron, and therefore, the products not only depend on the active sites on the TiO_2 surface but also on the species in solution [9]. The role of the active sites on TiO_2 is to generate the electrons necessary for reaction in Scheme 1 to proceed. Thus, the role of Cu^o is to restrain charge carriers recombination and to provide the sites for protons chemisorption. The latter may react with methoxy groups, $O\text{-}CH_3$, for instance, to produce methanol [12,24]. It can be observed in Table 1, entries 4 and 6, that with $Cu\text{-}TiO_2$ catalysts, methanol and multiple-carbon compounds are produced only when using aqueous alkaline solutions or when the catalyst consists of nanoalloys with metals like Pt, Au,

Rh, or mixed with oxides like CeO_2 [10,18,19]. Thus, in terms of methanol yield, the strategy that seems more promising is the use of alkaline solutions. In this sense, however, the effect of the large area-volume ratio characteristic of the optofluidic reactor used by [12] should not be overlooked. In this context, the advantages of using reactors where the photocatalytic area-volume is maximized have been demonstrated, specifically using capillary reactors. This has been conducted for both, photooxidation [27] and photoreduction [28] reactions. In this context, a variable affecting the production rate is if the catalyst is used as powder or as film. The latter leads to considerably higher production rates of both, H_2 and CH_4. Actually, the production rate of methane increases up to two orders of magnitude with respect to the analogous catalyst in powder [17]. Interestingly, the hydrogen production rate is not increased in the same extent as that of CH_4.

It is important to note that as specified in reaction Scheme 1, protons come from the solution, i.e., acids dissociation, and not from the water splitting reaction. This was demonstrated by adding a hole scavenger (sodium oxalate) [9]. Actually, it has been suggested that format is a source of protons not only for the reactions in Scheme 1 to proceed but also for the production of hydrogen [4]. Although format is not usually detected, this does not necessarily mean that is not formed.

As aforementioned, hydrogen evolution reaction by means of water reduction is undesirable because it limits the yield of the process toward other compounds. In this sense, it has been suggested that a strategy to restrain hydrogen evolution is by adjusting the content of copper [8]. A content of copper lower than 1% will favor the production of CO instead of H_2, since the adsorption energy of CO is higher than that of hydrogen. Oxygen should also be taken out of the reaction system since it is thought to quench the photogenerated electrons, and in consequence, a decay in the CO_2 photoconversion products is observed [17].

Regarding the catalyst, the following transformations are expected to occur,

$$Cu^o + h^+ \rightarrow CuO/Cu_2O + e^- \rightarrow Cu^o \quad (12)$$

$$CuO + e^- \rightarrow Cu_2O + O_2/H^+ \rightarrow CuO \quad (13)$$

An important variable that affects the final properties of the catalyst is the architecture of the supported nanoparticles. In order to modify this, the preparation method is of great importance [29]. As seen in Table 1, the applied preparation methods vary. From the reported ones, the chemical reduction is the most simple one since it can be conducted at room temperature and without the stage of calcination, and from a sustainability point of view, this method might be a promising one since this process does not imply as much energy as the thermal one where there is a high energy consumption during the calcination stage [30,31]. Nevertheless, the environmental impact derived from the use of energy coming from fossil fuels can be overcome by using renewable energy sources like solar or wind energy [32–34]. With this in mind, one can focus on the resulting chemical and physical characteristics attained by a specific synthesis method. In this sense, the use of H_2 to chemically reduce the copper species not only affects copper oxidation state but also titania surface by producing OH groups attached to the surface by hydrogen bridge bonds, thus producing Ti^{4+}-OH when the calcination temperature is above 400°C [17]. These hydroxylated sites and $Ti^{4+} - O^{2-}$ are believed to intervene in the following reactions [17,35],

$$Ti^{4+} - OH + CO_2 \rightarrow HCO_3^- \tag{14}$$

$$Ti^{4+} - O^{2-} + CO_2 \rightarrow CO_3^{2-} \tag{15}$$

Since the addition of Cu to TiO_2 has been shown to lead to increased yields of the products from CO_2 photoconversion, the Cu content has become an important variable to assess in this process. It has been demonstrated that more copper content does not imply higher yields toward CO and CH_4, and this has been ascribed to an aggregation of particles and to a light shield effect of excessive Cu [8,12]. Therefore, low copper content ($<1\%$) is recommended. When combined with other metals (Me), the ratio Cu/Me is an important parameter to be optimized since it directly impacts the product yield and selectivity [35].

Table 1 Studies on the CO_2 photoreduction catalyzed by Cu nanoparticles and alloys supported on TiO_2.

Entry	Preparation method	Particle size range (nm)	Reaction conditions	Phase	Production rate (μmol/g h)	Reference
1	Precipitation-calcination under H_2 atmosphere	4	Simulated sun light (150 W) Water vapor	Cu^+-Cu^o/TiO_2 3.04 eV	CO: 25 μmol/g CH_4: 4.4 μmol/g	[11]
2	Impregnation and calcination under H_2 atmosphere	5	UVC (8 W) Water vapor	1% Cu^o/TiO_2 (111)/(101) TiO_2	CO: 334 H_2: 452 CO: 160 H_2: 0.0	[4]
3	Solvothermal method	5–10	Xe lamp (300 W)	0.5 wt% Cu/TiO_2 TiO_2	CO: 32.5 H_2: 450 μmol/g CO: 6.2	[8]
4	Chemical reduction	7.85	Sodium oxalate (0.1 M) UVC (9OW)	30% Cu^o-TiO_2	H_2: 1690 μmol/g CO: 500 μmol/g CH_4: 90 μmol/g CH_3OH: 59.6 μmol/g C_3H_6O: 80.20 μmol/g CH_3COOH: 105.47 μmol/g C_3H_8O: 44.12 μmol/g	[9]
			H_2O UVC (9OW)	30% Cu^o-TiO_2	H_2: 27.40 μmol/g CO: 25.91 μmol/g CH_4: 6.15 μmol/g	

5	Airbrushing a catalytic ink onto porous carbon		1200 mW LED (365 and 450 nm) 0.5 M $KHCO_3$	Cu/TiO_2 UV Cu/TiO_2 VIS	CH_3OH: 230.3 CH_2O_2: 170 C_2H_5OH: 30 CH_3OH: 38 CH_2O_2: 8 C_2H_5OH: 30	[12]
6	Photo-induced reduction	Cu/Ag/TiO_2: ~20	Hg lamp 350–400 nm	TiO_2 Cu/TiO_2 Ag/TiO_2 Cu/Ag/TiO_2	CH_4: 1.5 CH_4: 4.5 CH_4: 1.8 CH_4: 7.1	[13]
7	Impregnation and reduction with H_2	4	Xe lamp (300 W) Gas phase, water vapor Simulated solar radiation Absorb in the red spectrum	TiO_2 nanosheets 0.5% Cu/TiO_2 nanosheets Ag/TiO_2 Cu-Ag/TiO_2	CO: 50 CH_4: 9.7 CO: 137 CH_4: 25 CO: 188 CH_4: 33 CO: 286 CH_4: 136	[7]
8	Electrodeposition	100	XeMg lamp (500 W)	Cu_2O/TiO_2	CH_3OH: identified but not quantified	[14]
9	Electrodeposition	Octahedral 150	Xe lamp (350 W) Visible light Simulated sun light Water vapor	Cu_2O/TiO_2 Band-gap: 2.0–2.2 eV	CH_4: 6250 μmol/L h	[15]

Continued

Table 1 Studies on the CO_2 photoreduction catalyzed by Cu nanoparticles and alloys supported on TiO_2—cont'd

Entry	Preparation method	Particle size range (nm)	Reaction conditions	Phase	Production rate (μmol/g h)	Reference
10	Photo-deposition (simulated sun-light)	0.5–3 (Av. 1.5)	Xe lamp (200 W)	TiO_2	H_2: 0.5 CO: 0.0 CH_4: 0.0 CH_3OH: 0.0	[6]
				Cu_2O/TiO_2	H_2: 2 CO: 0.0 CH_4: 0.0 CH_3OH: 0.0	
				Cu-Pt/TiO_2	H_2: 5 CO: 15 CH_4: 0 CH_3OH: 0.1	
11	Co-precipitation	20–50	Xe lamp (300 W)	Cu_2O	CH_4: 1.35	[16]
12	Deposition-precipitation	5	Xe lamp (150 W) Simulated sun light Water vapor	TiO_2	H_2: 2 CH_4: 0	[17]
				Cu/TiO_2	H_2: 16 CH_4: 40	
				Au/TiO_2	H_2: 34 CH_4: 32	
				(Au,Cu)/TiO_2	H_2: 16 CH_4: 44	
13	Solvothermal method and anodic oxidation	5–8	UV-Vis light (Xe lamp) Reducing agent: $N_2H_4{\cdot}H_2O$	Au_3 Cu@STO/TiO_2 (film)	CH_4: 421.2 C_2H_4, C_2H_6, C_3H_6: 304.2	[10]

14	Vacuum-thermal evaporation and condensation	5–20	UV radiation 5% H_2O/95% CO_2 Vis light	Cu_{50}-Rh_{50}	CH_3OH: 1.85	[18]
15	Impregnation of Cu^{2+} and Ce^{3+} and pyrolysis of MOF MIL-125-NH2	Cu (atomically dispersed)	Simulated solar light (Xe lamp) 320–850 nm	Cu/CeO_2-TiO_2	C_2H_4: 4.51 CH_4: 1.5 CO: 3.65	[19]

NR, not reported.

It can also be observed in Table 1 that Cu is added to the TiO_2 also as Cu_2O. The anchoring of Cu_2O to the TiO_2 surface brings the following advantages under sun-light simulated irradiation:

- Hole-electron pairs are generated in both semiconductors, TiO_2 and Cu_2O [15,16].
- Shifts the absorption edge of TiO_2 from 389 to 800 nm [16].
- Charges recombination is reduced [15,16].
- The oxidation potential of photo-generated holes is reduced (this exerts a similar effect than the use of sacrificial agents, i.e., methanol, glycerol) [15].

Fig. 6 illustrates the CO_2 photoreduction catalyzed by Cu_2O/TiO_2. In this figure, the energy levels for both semiconductors are depicted. In this case, a *p-n* heterojunction is produced since Cu_2O and TiO_2 are *p*-type and *n*-type semiconductors, respectively [16]. In this way, an efficient separation of photo-generated charge carriers is expected. This has been demonstrated to be advantageous in other types of photocatalytic reactions such as hydrogen production from water splitting. For these materials to be efficient, the well-aligned band edges of TiO_2 and Cu_2O are key [15].

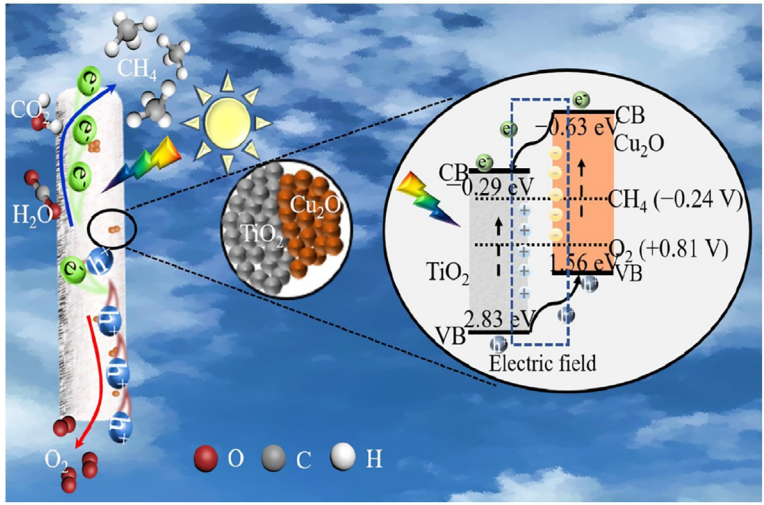

Fig. 6 Illustration of CO_2 photoreduction catalyzed by Cu_2O/TiO_2. *(Credit: Reprinted from G. Yang, P. Qiu, J. Xiong, X. Zhu, G. Cheng, Facilely anchoring Cu2O nanoparticles on mesoporous TiO2 nanorods for enhanced photocatalytic CO2 reduction through efficient charge transfer, Chin. Chem. Lett. (2022), https://doi.org/10.1016/j.cclet.2021.10.047 with permission from Elsevier.)*

As can be seen in Table 1, when decorating TiO_2 with Cu_2O, the main reported formed products are methanol [14], hydrogen [6], and methane [15,16]. During the photocatalytic process, the Cu_2O is oxidized toward CuO by transferring electrons from its conduction band to the TiO_2 conduction band [6].

Finally, there are the catalysts where copper is combined with other elements like Ag, Pt, Au, Rh, and Co. This combination leads to changes in optical and electronic properties, reflected in different catalytic activities and therefore product yield and selectivity. Take as an example, entry 6 in Table 1, where it can be observed that the combination with silver increases the hourly production of methane with respect to copper or silver alone. The production of carbon monoxide is also increased albeit at different extent than methane. This has been attributed to the surface plasmonic resonance effect (SPR) of silver, located at 420–450 nm [13,36], that results in visible light absorption enhancement that translates in an increased electron flow from silver to the TiO_2 conduction band, and these electrons migrate to Cu and reduce the already adsorbed CO_2 [7]. Thus, in this case, electrons generation is photo-induced on silver and TiO_2. When these electrons are transferred to copper, they are available to conduct the reactions depicted in Scheme 2 [7]. According to this reaction scheme and as in the above discussed studies, the first steps are the generation of electrons and the adsorption of carbon dioxide onto copper, then the transfer of electrons begins producing the carbon dioxide radical anion $CO_2^{\bullet-}$ that can react with hydroxyl radicals to produce bicarbonate anions and can also react with another carbon dioxide radical anion to produce carbonate anions. These two chemisorbed species are then reduced by the addition of protons and electrons until methane is formed [7]. The preferred form of adsorption is bidentate carbonate ($b-CO_3^-$). This suggests that the reduction of CO_2 occurs at the photocatalytic surface. This is controversial since there are works that suggest HCO_3 being the specie that is adsorbed and transformed into valuable chemicals.

The aforementioned supports the fact that the methane production rate will be impacted by the composition of the metallic particles on the TiO_2 surface [13].

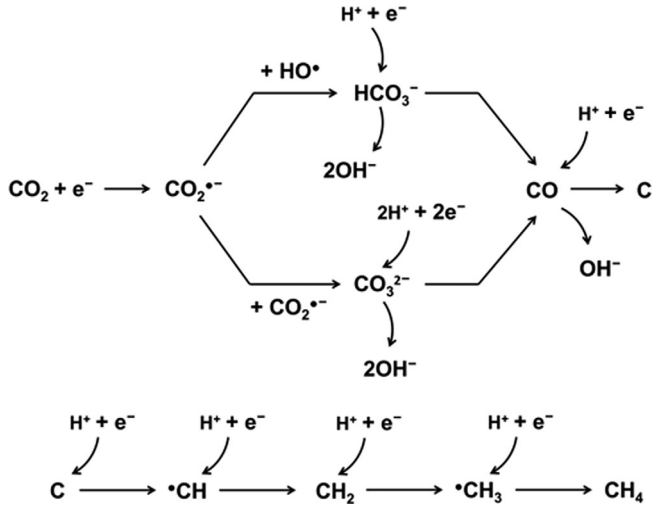

Scheme 2 Reaction pathway to produce carbon monoxide and methane by the CO_2 photoreduction catalyzed by Ag/Cu-TiO_2. *(Credit: Own elaboration.)*

The addition of other species, such as CeO_2, results in an improvement of CO_2 adsorption compared to TiO_2 added only with Cu [19]. In this type of material, where Cu is atomically dispersed, the production of ethylene has been reported [19] to proceed via the following mechanism:

$$H_2O \rightarrow H^+ + OH^- \tag{16}$$

$$^* + CO_2 + e^- (\rightarrow {}^*CO_2-) + H^+ \rightarrow {}^*COOH \tag{17}$$

$$^*COOH + e^- + H^+ \rightarrow {}^*CO + H_2O \tag{18}$$

$$^*CO + {}^*CO \rightarrow {}^*COCO \tag{19}$$

$$^*COCO + 8e^- + 8H^+ \rightarrow C_2H_4 + 2H_2O \tag{20}$$

$$2OH^- + 2h^+ \rightarrow H_2O_2 \tag{21}$$

In this case, $Cu^{\delta+}$ $(0 < \delta < 1)$ has been proven to be the active sites necessary for the C-C coupling between adjacent chemisorbed CO molecules [37]. It is also interesting to note that the production of H_2O_2 is acknowledged. In the context of chemical reduction, this is as a drawback, since the combination of a transition metal with light and hydrogen peroxide is excellent to conduct oxidation reactions via a photo-Fenton like mechanism (Cu and light catalyze the H_2O_2 dissociation into hydroxyl radicals [38,39], which practically

"burn" any organic compound due to its high oxidation power, 2.8 V). Thus, this fact might lead to the decrease in the organic molecules yield.

The yield decrease of the formed organic compounds has been documented in other works and is also ascribed to the formed oxygen [13]. Methane, however, accumulates because its oxidation is unlikely [13].

Methanol was also observed when Rh is combined with Cu in a 50–50 ratio (entry 13, Table 2). It is worth noticing that Rh improves the dissociation of CO_2. One problem with using Rh, though, is that it oxidizes and loses activity. In the nanoalloy Cu-Rh, Cu is believed to act as a sacrificial anode thus limiting Rh oxidation [18].

When copper is combined with platinum (entry 10, Table 1), the production of carbon monoxide and methanol is enhanced compared to that using Cu_2O alone [6]. Actually, CO appears when Pt is added in the system studied by Liu et al. [6], and it increases about 40% when a solution of sodium bicarbonate is used instead of only water. Fig. 7 depicts the photo-generated carriers when adding Pt to a Cu/TiO_2 catalyst and also having the presence of cuprous oxide on the TiO_2 surface, in such a way that the catalytic system $Cu\text{-}Pt/TiO_2\text{-}CuO$ is produced. This system exhibits two types of sites: Cu-Pt for electron capture to conduct reduction reactions like CO_2 photoconversion and CuO for holes capture to conduct oxidation reactions like water splitting. In this sense, it has been postulated that the oxidation ability of the catalyst determines the extent of the photocatalytic CO_2 reduction by water [51,52]. The main disadvantages of adding Pt are price, availability, and that it deactivates with CO.

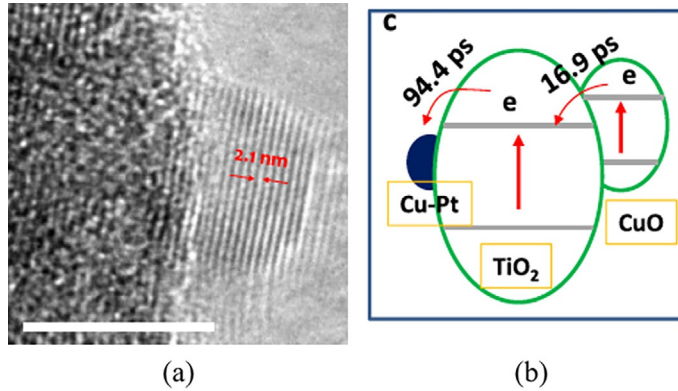

Fig. 7 Cu-Pt/TiO_2-CuO: (A) HRTEM. (B) Photo-generated carriers migration. *(Adapted from J. Liu, M. Liu, X. Yang, H. Chen, S.F. Liu, J. Yan, Photo-redeposition synthesis of bimetal Pt-Cu co-catalysts for TiO2 photocatalytic solar-fuel production. ACS Sustain. Chem. Eng. 8 (2020) 6055–64, https://doi.org/10.1021/acssuschemeng.0c00969 with permission from the American Chemical Society.)*

Another element that has been widely used in monometallic form or in combination with copper is gold. As seen in Table 1, this combination promotes the selectivity toward H_2 and CH_4, and the photo-response is also enhanced. Fig. 8 depicts the effect of irradiation wavelength on the surface phenomena that leads to different product distributions. When wavelength is smaller than 380 nm, i.e. UV light, the expected excitation of one e^- from the valence band to the conduction band in anatase occurs. This electron is then captured by the nanoalloy, thus promoting hydrogen generation and CO_2 reduction. When only visible light is used, the electrons are generated by the plasmonic effect of Au, in a similar fashion than with Ag, and they can be excited toward the conduction band of anatase, thus electrons are available for reaction at the metallic nanoparticles and at the titania surface. Nevertheless, the generated electrons prefer to reduce oxidized copper than migrate to the conduction band of titania [17]. It is important to note that CH_4 was only observed under Vis light. H_2 was observed at both

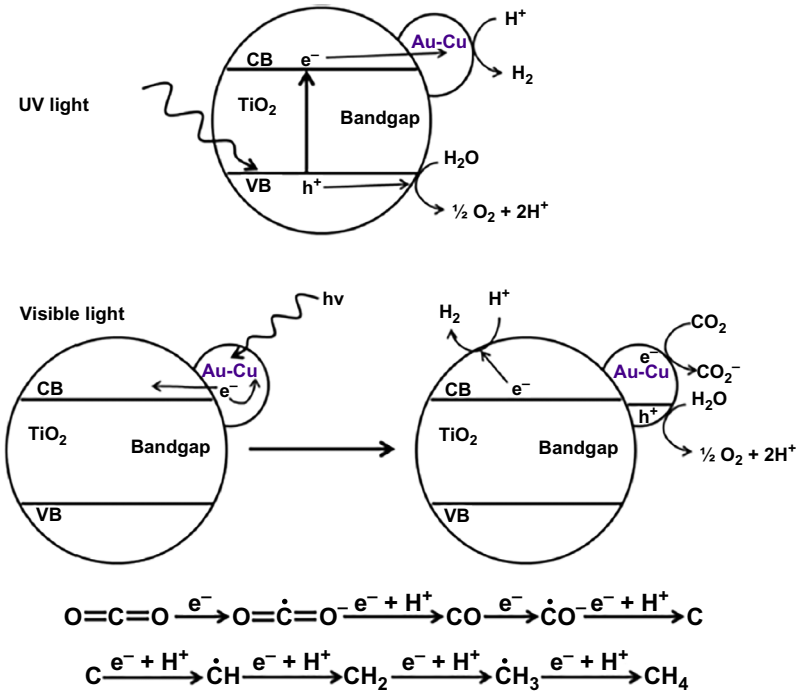

Fig. 8 Effect of the irradiation wavelength on product distribution of CO_2 photoreduction catalyzed by Au-Cu/TiO_2 and proposed route for methane formation. *(Reprinted with permission from S. Neatu, J.A. Maciá-Agullò, P. Concepciòn, H. Garcia, Gold-copper nanoalloys supported on TiO2 as photocatalysts for CO2 reduction by water, J. Am. Chem. Soc. 136 (2014) 15969–76, https://doi.org/10.1021/ja506433k, American Chemical Society.)*

wavelengths, at different rates though [17]. Fig. 8 also depicts the plausible methane generation pathway that coincides with the carbene-type pathway [53]. It is worth noting that CO desorption is favored in gold since the activation energy of this step is lower than in copper, 38 and 65 kJ/mol, respectively [10,54,55]. To activate the CO desorption from Cu, the use of highly energetic lamps is recommended.

In summary, it can be said that metallic nanoalloys allow the electrons transfer between metals [10,17,56] and limit the electrons backflow to the semiconductor [10]. When using nanoalloys, the ratio of metals also impacts the product distribution and thus the selectivity. Thus, special care should be taken on optimizing such a ratio.

An opportunity area to improve the yield toward methane, for example, is the use of different reducing agents to water. In this context, hydrous hydrazine ($N_2H_4{\cdot}H_2O$) has been proven to be an alternative as it increases methane production rate up to seven times with respect to water and inhibits catalyst deactivation [10]. This source of protons also allows the production of C2 and C3 compounds, i.e., C_2H_6, C_2H_4 and C_3H_6, through a dimerization-based mechanism that acknowledges the following steps [10]:

(1) CO_2 adsorption and reduction
(2) Generation of protons from $N_2H_4{\cdot}H_2O$
(3) Dimerization
(4) Dimer further reduction
(5) Methyl addition and further reduction
(6) Dehydration

The effect of the nanoarchitecture of both, catalyst and support, has been evidenced through different works. From these studies, it can be concluded that nanotube arrays of titania, electrochemically obtained, importantly enhance the production carbon compounds [10].

2.2 CO_2 photoconversion catalyzed by gold nanoparticles on TiO_2

Gold (Au) is a noble metal that is usually inert to a variety of molecules; this, however, changes with the right size (nanometric) and with the proper support [57]. The studies related to CO_2 photoconversion catalyzed by Au NPs/TiO_2-based catalysts are summarized in Table 2. An important characteristic of this noble metal to conduct the mentioned process is its reactivity toward carbon monoxide and oxygen at low temperature [57].

According to the results summarized in Table 2, there are various methods that have been assessed to obtain nanometric gold. Within these procedures, the one that allows synthesizing the smallest gold particles is

the precipitation method (entries 6, 7 and 10). This method allows obtaining Au NPs as small as 1.9 nm [45]. Briefly, in this procedure, an aqueous solution of $HAuCl_4 \cdot 3H_2O$ with a suitable concentration of Au is adjusted to a pH of 6–10 (usually with urea), and subsequently, TiO_2 is added under vigorous stirring for 2 h at 70°C. The mixture is kept under stirring overnight, and finally, the solid is filtered, dried at 100°C, and calcined at 200°C for 4 h [45]. The precipitation pH directly affects the particle diameter of Au. Below pH 4, $AuCl_4^-$ ion is formed and this leads to particle size between 5 and 20 nm; while above pH 6, the predominant gold specie is $Au(OH)_nCl_{4-n}$ and it is worth noting that the effect is not as significant and a particle size lower than 5 nm is expected [57]. There are some variants of this method in the temperature at which precipitation is conducted; 90°C can be used instead of using 70°C and also reaction time than can vary between 2 and 4 h. Calcination also may range between 200°C and 400°C [17,44–46].

Another commonly used method to nanoparticles synthesis is by chemical reduction. This is a rather simple method, where a metallic salt is dissolved in an aqueous dispersion of the support and a reducing agent like $NaBH_4$ is added [58]. An advantage of this method is that usually eliminates the stage of calcination [59]. Nevertheless, in the case of gold NPs synthesis, a more complex method based on reduction with $NaBH_4$ has been applied [40]. In such a study, in a typical synthesis, a solution of noble metal precursors was incorporated into the support in Au/Pd weight ratios of 3, 1, and 1/3. The mixture was then fed to a membrane reactor concomitantly with a $NaBH_4$ solution and under H_2 flow. As the $NaBH_4$ was consumed, more hydrogen gas was bubbled into the reactor. Finally, the material was filtered, dried, and calcined at 400°C. The AuPd nanoparticles exhibited high dispersion on the support surface with AuPd particle sizes of 3.3–3.9 nm. The samples presented surface areas of 60 m^2/g, porosity of 90%, presence of anatase/rutile phases with crystal sizes around 20 nm and absorption bands in the visible region at 530 nm. Au^0, Au^+, and Au^{+3} species were identified in the materials by XPS analysis. An important characteristic of this material was the architecture of the utilized TiO_2, a three-dimensionally ordered macroporous, also known as inverse opals that are known to improve light harvesting [40,60,61]. This has also been applied by Wei et al., who obtained Au@CdS nanoparticles on inverse opal TiO_2 using the reported methodology in [41]. The nanoparticles were well dispersed on the inner wall of the support with different Au/Cd molar ratios. The Au loading in the material was 3–3.3 wt%. The solid exhibited an anatase structure with a crystal size around 20 nm. The size of the Au particle was 3.5 nm and the material

presented surface areas between 51 and 54 m^2/g. Absorption in the visible light region (450–650 nm) was observed.

Impregnation is not usually a recommended method to obtain Au NPs because it is not related to a high Au dispersion, unlike with other metals like Pd or Pt [57].

Khaletskaya et al. synthesized Au nanoparticles supported on the TiO_2 surface through the pyrolysis of Au/NH_2-MIL-125 (Ti-containing metal-organic structure) nanocrystals [50]. The metal-organic structure was treated by pyrolytic decomposition at 450°C under oxygen for 2 h to obtain the Au/TiO_2 material. The solid exhibited a combination of anatase-rutile crystal phases and a surface area of 19.8 m^2/g. Au nanoparticles were found distributed on the support.

Other procedure is the pulsed anodization technique used by Zeng et al. [22] to obtain TiO_2 nanotubes. Once obtained, the gold nanoparticles are deposited by magnetron sputtering without substrate heating. The position rate was 7.4 nm/min at a chamber pressure of 7 mTorr. The loading of the nanoparticles was estimated at 85 μg per sample. Finally, the samples were annealed in a tube furnace at 525°C for 30 min. The prepared material showed anatase/rutile phases with gold nanoparticles (diameters ranging from 3 to 7 nm) homogeneously distributed on the TiO_2 walls.

In all cases shown in Table 2, the absorbance band of the synthesized catalysts varies between 450 and 700 nm. This means that can be used to conduct reactions under Vis light. Because there is TiO_2 in the catalyst, however, it is recommended to use the whole sun-light spectrum because TiO_2 is excited by wavelengths lower than 380 nm. The intensity of the absorbance band relates to both, particle size and metallic content [59].

In the studies related to the application of Au nanoparticles/TiO_2 to photo-catalyze the CO_2 conversion, the main identified products have been CO, CH_4, and H_2. Depicted in Fig. 9 is the production rate of these compounds as a function of the assessed catalyst. These studies were conducted by different research groups around the globe and therefore under different reaction conditions; thus, this figure intends to visually show what catalyst leads to the highest production rate of each of the above-mentioned gases. The outcome should be taken care, since in some cases, the results are not necessarily by the effect of the catalyst but by the effect of the electron donor. The results for methane were split into two graphs, Fig. 9A and B, according to the corresponding value. The values higher than 50 μmol/g h are in Fig. 9B. All the results plotted in Fig. 9 were the maximum reported by references listed in Table 2.

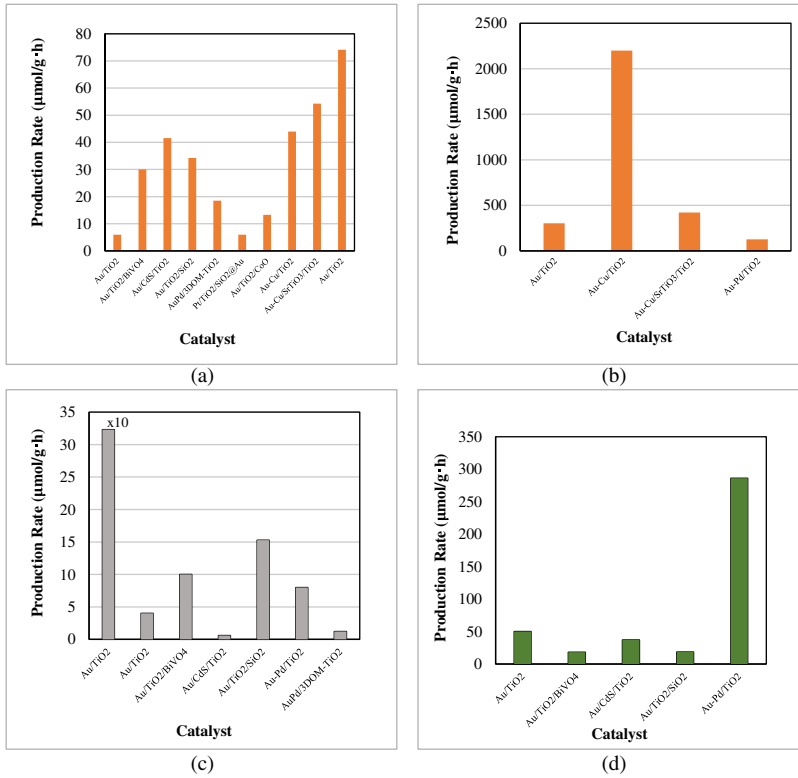

Fig. 9 Effect of type of catalyst on production rate of (A) and (B) methane, (C) carbon monoxide, (D) hydrogen.

In the context of CH_4 production, it can be observed in Fig. 9A that most of the assessed catalysts lead to methane production rates lower than 100 μmol/gh. It can also be observed in Fig. 9B that the highest production rate (2200 μmol/gh) is obtained with the Au-Cu/TiO_2 catalyst (entry 9, Table 2). The peculiarity of this catalyst is being coated as film instead of being used as powder, and therefore, the main reason for the high production rate is the large area/volume ratio. Another key parameter is the ratio Au/Cu. For the results shown in Fig. 9, an Au/Cu ratio of 2/1 was used. This catalyst used as powder also outstands in the production of methane since this was obtained at a rate of 44 μmol/gh (see Fig. 9B). The catalyst was obtained by deposition-precipitation and the resulting Au-Cu/TiO_2 material presented a good distribution of Au-Cu nanoparticles with average particle sizes of 5 nm. The material was prepared in two stages: in the first one Au was loaded on the titania by means of an aqueous solution

of $HAuCl_4$ adjusting the pH to 8.5, then it was stirred for 5 h at 75°C, filtered, washed, dried under vacuum at 80°C, and calcined at 400°C for 2 h. In the second stage, the obtained Au/TiO_2 powder is added to an aqueous solution of $Cu(NO_3)_2$ and then the same steps for gold deposition were followed [17]. It has been postulated that for this catalyst the photoreduction begins with the absorption and distribution of reactive species (CO_2 and H_2O), generation of the e^-/h^+ pair, and CO_2 activation by one electron to form surface $CO_2^{\bullet-}$. Subsequently, the reduction is carried out by a series of steps that involve the h^+/e^- transfer, which leads to the formation of C-H bonds through the cleavage of C—O bonds [17].

Another system that has reported improvements on CH_4 production rate is the catalyst $Au\text{-}Cu/SrTiO_3/TiO_2$ (entry 1, Table 2). At this point, it is worth noting that $SrTiO_3$ was the first catalyst to be tested in the photocatalytic reduction of CO_2 in 1978 by Somorjai's group [22,62]. By using $Cu/SrTiO_3/TiO_2$, a CH_4 production rate of 421 μmol/g h has been obtained [10], albeit with a reducing agent different to water, i.e., hydrous hydrazine ($N_2H_4H_2O$). With water, the methane production rate was 54.3 μmol/g h, which is the second highest when using water as electron donor. Both results were obtained with a 0.75% of gold, which was not the highest assessed content. This highlights the importance of optimizing the ration Au/Cu. This catalyst was prepared by a microwave-assisted solvothermal method. An important step in this method is the removal of residual carbon from the surface by calcination at 500°C. The resulting material exhibited nanotube array morphology, with a uniform distribution of the Au-Cu species on the support (nanoparticle size of 5.14–7.78 nm), as well as the presence of anatase crystalline phase and an absorbance band at 570 nm. It is important to mention that in the referred study, it was established that the content of Au promotes the formation of hydrocarbons instead of CO. This has been ascribed to the lower adsorption energy of CO on gold than in copper. Another important result is the fact that the change of reducing agent exerts a greater impact on hydrocarbons production than the addition of $SrTiO_3$, for instance.

Regarding CO, it can be observed in Fig. 9C that the best results in terms of production rate were obtained when using the system $Au/TiO_2/SiO_2$ (entry 10, Table 2). In this material, TiO_2 nanospheres were grown on silica and then Au nanoparticles were loaded. To achieve so, the catalyst was prepared [47] by dispersing TiO_2/SiO_2 in water with ultrasound and with a solution of $HAuCl_4{\cdot}4H_2O$ (1 wt%) and urea. The suspension was vigorously stirred at 90°C for 4 h and then the solid was separated by

centrifugation, washed with ultrapure water, dried at 80°C under vacuum, and calcined at 300°C in air. The resulting material showed a uniform and well-dispersed loading of the Au nanoparticles with the particles size ranging 3–5 nm. The TiO_2 presented the characteristic anatase phase. The experiments with this material were conducted under simulated sunlight (300 W Xe lamp) and a CO_2/H_2O stream. The obtained CO production rate with this catalyst was ca. 15 μmol/g h. However, when using Cu/$SrTiO_3/TiO_2$, one can achieve a CO production rate two orders of magnitude higher than that reported by [47]. This should not only be ascribed to the different catalyst solely but also to the use of an electron donor different to water, i.e., hydrous hydrazine. The actual CO production rate with this catalyst was 3770 μmol/g h [10]. This result is not shown in Fig. 9 because its magnitude did not allow a proper observation of the other results.

Other promising results were those obtained by Zeng et al. [22]; the obtained production rates for CH_4 and CO were 302 and 323 μmol/g h, respectively. The used catalyst was Au/TiO_2. In this work as in the others catalyzed by metal particles, the methane is expected to be produced by either a carbene- or formaldehyde-type mechanism [22,53].

3. Concluding remarks

Low selectivity and the competing reaction of hydrogen evolution are two problems in CO_2 photoconversion. This will depend on the type of nanocatalyst, catalyst and support nanoarchitecture, reducing agent and irradiation wavelength. The addition of copper or gold nanoparticles to the TiO_2 surface enhances the production rate of carbon monoxide and methane. These rates have achieved three orders of magnitude in both cases. Such a production rate is only achieved when gold and copper are combined into an alloy nanoparticle at the TiO_2 surface and when another than water electron donor is used. With water only and with a single metal on the semiconductor surface, copper outperforms gold and the production rate of both, carbon monoxide and methane, falls to two orders of magnitude. A relative high production rate is also obtained when films instead of powders are used.

One of the factors responsible for the enhancement in production rates is that the charge carriers' recombination is inhibited by the addition of metallic nanoparticles or nanoalloys. When using nanoalloys, however, the ratio of metals also impacts the product distribution and thus selectivity.

Table 2 Preparation method and properties of catalysts based on TiO_2-supported Au nanoparticles.

Entry	Preparation method	Catalyst	Au content (particle size)	Crystalline phase	Surface area	Optical properties	Reference
1	Solvothermal	Au-Cu/$SrTiO_3$/TiO_2	0.4 wt% (5.14–7.78 nm)	Anatase	–	Absorbance band at 570 nm	[10]
2	Chemical reduction	AuPd/3DOM-TiO_2	0.9–3.4 wt% (3.3–3.9 nm)	Anatase/rutile	60 m^2/g	Absorbance peak at 530 nm	[40]
3		Au/CdS/TiO_2	3.0–3.3 wt% (3.5 nm)	Anatase	51–54 m^2/g	Absorbance: 450–650 nm	[41]
4	Deposition	Au/TiO_2/CoO	Mass ratio: 0.5–5.0	Anatase	31.1 m^2/g	Absorbance peak at 554 nm	[42]
5		Au-Pd/TiO_2	2.3 wt% (5 nm)	Anatase	306 m^2/g	Absorbance peak at 532	[43]
6	Deposition-precipitation	Au/TiO_2	1 wt% (3 nm)	Anatase	–	Absorbance peak at 604 nm	[44]
7		Au/TiO_2	0.5–3.0 wt% (1.9–3 nm)	Anatase	111.1–122.7 m^2/g	Absorbance band: 450–600 nm	[45]
8		Au/TiO_2	0.097–1.054 wt% (10.8 nm)	Anatase	32.47–63.67 m^2/g	–	[46]
9		Au-Cu/TiO_2	Au/Cu weight ratio: 1/2, 2/1 (5 nm)	Anatase/rutile	–	–	[17]
10		Au/TiO_2/SiO_2	1 wt% (3–5 nm)	Anatase	–	–	[47]
11		Pt/TiO_2/SiO_2@Au	(4–26 nm)	Anatase/rutile	–	Absorbance peak at 530 nm	[48]
12	Wet chemical	Au/TiO_2/$BiVO_4$	Au/$BiVO_4$ molar ratio: 2% (10 nm)	Anatase	11.6 m^2/g	Absorbance band at 660 nm	[49]
13	Pyrolysis	Au/TiO_2	39.1 mg of precursor	Anatase/rutile	19.8 m^2/g	–	[50]
14	Pulsed anodization	Au/TiO_2	85 μg per sample (3–7 nm)	Anatase/rutile	–	Absorbance band: 350–550 nm	[22]

Regarding the effect of the radiation source wavelength, methane is not observed with only UV light. Besides, TiO_2 is subutilized when only Vis-light is applied.

The deactivation of copper-based catalysts is ascribed to the oxidation of metallic copper when water is used as reducing agent, also to the carbon monoxide chemisorption. If an energetic enough lamp is not utilized, then the CO desorption is not activated thus limiting or even inhibiting the whole process.

The strategies that have worked to improve the effectiveness of photocatalysts in the CO_2 reduction are use of nanotube arrays of TiO_2, development of heterostructures to improve charge separation, use of nanoallys, using films instead of powders, using electron donors different to water, and the use of the whole sun-light spectrum. It is advised to remove O_2 from the reaction systems, using a selective membrane perhaps. Little work has been conducted related to the effect of textural and physicochemical properties like amount and strength of acid and basic sites on the catalytic surface.

Acknowledgments

The financial support of CONACYT is acknowledged. The technical support of Osmin Aviles-Garcia and Vianey Facio Arce in the digitalization process is also acknowledged.

References

[1] A.V. da Rosa, J.C. Ordóñez, Hydrogen production, in: Fundamentals of Renewable Energy Processes, Elsevier, 2022, pp. 419–470, https://doi.org/10.1016/B978-0-12-816036-7.00021-X.

[2] P. Basu, Introduction, in: Biomass Gasification, Pyrolysis and Torrefaction: Practical Design and Theory, Elsevier, 2018, pp. 1–27, https://doi.org/10.1016/B978-0-12-812992-0.00001-7.

[3] A.A. Tountas, X. Peng, A.v. Tavasoli, P.N. Duchesne, T.L. Dingle, Y. Dong, et al., Towards solar methanol: past, present, and future, Adv. Sci. (2019) 6, https://doi.org/10.1002/advs.201801903.

[4] N. Singhal, A. Ali, A. Vorontsov, C. Pendem, U. Kumar, Efficient approach for simultaneous CO and H2 production via photoreduction of CO2 with water over copper nanoparticles loaded TiO2, Appl. Catal. A Gen. 523 (2016) 107–117, https://doi.org/10.1016/j.apcata.2016.05.027.

[5] P. Akhter, M. Hussain, G. Saracco, N. Russo, Novel nanostructured-TiO2 materials for the photocatalytic reduction of CO2 greenhouse gas to hydrocarbons and syngas, Fuel 149 (2015) 55–65, https://doi.org/10.1016/j.fuel.2014.09.079.

[6] J. Liu, M. Liu, X. Yang, H. Chen, S.F. Liu, J. Yan, Photo-redeposition synthesis of bimetal Pt-Cu Co-catalysts for TiO2 photocatalytic solar-fuel production, ACS

Sustain. Chem. Eng. 8 (2020) 6055–6064, https://doi.org/10.1021/acssuschemeng.0c00969.
[7] N. Li, D. Geng, J. Zhou, Ag and Cu nanoparticles synergistically enhance photocatalytic CO_2 reduction activity of B phase TiO_2, Catal. Lett. 152 (2022) 124–138, https://doi.org/10.1007/s10562-021-03618-4.
[8] Y. Lan, Y. Xie, J. Chen, Z. Hu, D. Cui, Selective photocatalytic CO2 reduction on copper-titanium dioxide: a study of the relationship between CO production and H2 suppression, Chem. Commun. 55 (2019) 8068–8071, https://doi.org/10.1039/c9cc02891a.
[9] J.A. Torres, J.C. da Cruz, A.E. Nogueira, G.T.S.T. da Silva, J.A. de Oliveira, C. Ribeiro, Role of Cu0-TiO2 interaction in catalyst stability in CO2 photoreduction process. Journal of environmental, Chem. Eng. (2022) 10, https://doi.org/10.1016/j.jece.2022.107291.
[10] Q. Kang, T. Wang, P. Li, L. Liu, K. Chang, M. Li, et al., Photocatalytic reduction of carbon dioxide by hydrous hydrazine over Au-Cu alloy nanoparticles supported on $SrTiO_3/TiO_2$ coaxial nanotube arrays, Angew. Chem. Int. Ed. 54 (2015) 841–845, https://doi.org/10.1002/anie.201409183.
[11] L. Liu, F. Gao, H. Zhao, Y. Li, Tailoring Cu valence and oxygen vacancy in Cu/TiO2 catalysts for enhanced CO2 photoreduction efficiency, Appl. Catal. B Environ. 134–135 (2013) 349–358, https://doi.org/10.1016/j.apcatb.2013.01.040.
[12] J. Albo, M.I. Qadir, M. Samperi, J.A. Fernandes, I. de Pedro, J. Dupont, Use of an optofluidic microreactor and Cu nanoparticles synthesized in ionic liquid and embedded in TiO2 for an efficient photoreduction of CO2 to methanol, Chem. Eng. J. (2021) 404, https://doi.org/10.1016/j.cej.2020.126643.
[13] M.L. Ovcharov, V.V. Shvalagin, V.M. Granchak, Photocatalytic reduction of CO2 on mesoporous TiO2 modified with Ag/Cu bimetallic nanostructures, Theor. Exp. Chem. 50 (2014), https://doi.org/10.1007/s11237-014-9362-x.
[14] J. Wang, G. Ji, Y. Liu, M.A. Gondal, X. Chang, Cu2O/TiO2 heterostructure nanotube arrays prepared by an electrodeposition method exhibiting enhanced photocatalytic activity for CO2 reduction to methanol, Catal. Commun. 46 (2014) 17–21, https://doi.org/10.1016/j.catcom.2013.11.011.
[15] Y. Li, W. Zhang, X. Shen, P. Peng, L. Xiong, Y. Yu, Octahedral Cu2O-modified TiO2 nanotube arrays for efficient photocatalytic reduction of CO2, Chin. J. Catal. 36 (2015) 2229–2236, https://doi.org/10.1016/S1872-2067(15)60991-3.
[16] G. Yang, P. Qiu, J. Xiong, X. Zhu, G. Cheng, Facilely anchoring Cu2O nanoparticles on mesoporous TiO2 nanorods for enhanced photocatalytic CO2 reduction through efficient charge transfer, Chin. Chem. Lett. (2022), https://doi.org/10.1016/j.cclet.2021.10.047.
[17] S. Neatu, J.A. Maciá-Agullò, P. Concepciòn, H. Garcia, Gold-copper nanoalloys supported on TiO2 as photocatalysts for CO2 reduction by water, J. Am. Chem. Soc. 136 (2014) 15969–15976, https://doi.org/10.1021/ja506433k.
[18] L. Sorokina, A. Savitskiy, O. Shtyka, T. Maniecki, M. Szynkowska-Jozwik, A. Trifonov, et al., Formation of Cu-Rh alloy nanoislands on TiO2 for photoreduction of carbon dioxide, J. Alloys Compd. (2022) 904, https://doi.org/10.1016/j.jallcom.2022.164012.
[19] T. Wang, L. Chen, C. Chen, M. Huang, Y. Huang, S. Liu, et al., Engineering catalytic interfaces in Cu δ+/CeO 2-TiO_2 Photocatalysts for synergistically boosting CO_2 reduction to ethylene, ACS Nano 16 (2022) 2306–2318, https://doi.org/10.1021/acsnano.1c08505.
[20] L. Liu, Y. Li, Understanding the reaction mechanism of photocatalytic reduction of CO2 with H2O on TiO2-based photocatalysts: a review, Aerosol Air Qual. Res. (2014) 14, https://doi.org/10.4209/aaqr.2013.06.0186.

[21] N.M. Dimitrijevic, B.K. Vijayan, O.G. Poluektov, T. Rajh, K.A. Gray, H. He, et al., Role of water and carbonates in photocatalytic transformation of CO_2 to CH4 on titania, J. Am. Chem. Soc. 133 (2011) 3964–3971, https://doi.org/10.1021/ja108791u.
[22] S. Zeng, E. Vahidzadeh, C.G. Van Essen, P. Kar, R. Kisslinger, A. Goswami, et al., Optical control of selectivity of high rate CO2 photoreduction via interband- or hot electron Z-scheme reaction pathways in Au-TiO2 plasmonic photonic crystal photocatalyst, Appl. Catal. B Environ. (2020) 267, https://doi.org/10.1016/j.apcatb.2020.118644.
[23] J.P. Espinós, J. Morales, A. Barranco, A. Caballero, J.P. Holgado, A.R. González-Elipe, Interface effects for Cu, CuO, and Cu2O deposited on SiO2 and ZrO2. XPS determination of the valence state of copper in Cu/SiO2 and Cu/ZrO2 catalysts, J. Phys. Chem. B 106 (2002) 6921–6929, https://doi.org/10.1021/jp014618m.
[24] J.A. Torres, J.C. da Cruz, A.E. Nogueira, G.T.S.T. da Silva, J.A. de Oliveira, C. Ribeiro, Role of Cu0-TiO2 interaction in catalyst stability in CO2 photoreduction process, J. Environ. Chem. Eng. (2022) 10, https://doi.org/10.1016/j.jece.2022.107291.
[25] R. Peña, L. Hurtado, R. Romero, R. Natividad, Absorption and reaction of CO2 in capillaries, in: CIERMMI Women in Science Engineering and Technology TXV, 2021, pp. 51–74, https://doi.org/10.35429/h.2021.6.51.74.
[26] Ş. Neaţu, J.A. Maciá-Agulló, H. Garcia, Solar light photocatalytic CO2 reduction: general considerations and selected bench-mark photocatalysts, Int. J. Mol. Sci. (2014) 15, https://doi.org/10.3390/ijms15045246.
[27] L. Hurtado, D. Solís-Casados, L. Escobar-Alarcón, R. Romero, R. Natividad, Multiphase photo-capillary reactors coated with TiO2 films: preparation, characterization and photocatalytic performance, Chem. Eng. J. 304 (2016) 39–47, https://doi.org/10.1016/j.cej.2016.06.003.
[28] L. Hurtado, R. Natividad, H. García, Photocatalytic activity of Cu2O supported on multi layers graphene for CO2 reduction by water under batch and continuous flow, Catal. Commun. 84 (2016) 30–35, https://doi.org/10.1016/j.catcom.2016.05.025.
[29] X. Liu, J. Iocozzia, Y. Wang, X. Cui, Y. Chen, S. Zhao, et al., Noble metal-metal oxide nanohybrids with tailored nanostructures for efficient solar energy conversion, photocatalysis and environmental remediation, Energy Environ. Sci. 10 (2017) 402–434, https://doi.org/10.1039/c6ee02265k.
[30] A. Rahman, S. Kang, S. McGinnis, P.J. Vikesland, Life cycle impact assessment of iron oxide (Fe3O4/γ-Fe2O3) nanoparticle synthesis routes, ACS Sustain. Chem. Eng. 10 (2022) 3155–3165, https://doi.org/10.1021/acssuschemeng.1c05763.
[31] F. Wu, Z. Zhou, A.L. Hicks, Life cycle impact of titanium dioxide nanoparticle synthesis through physical, chemical, and biological routes, Environ. Sci. Technol. 53 (2019) 4078–4087, https://doi.org/10.1021/acs.est.8b06800.
[32] V. Arundhathi, S.N. Manasa, S.K. Lakshmi, V. Varsha, B. Sundaram, Life-cycle assessment of various synthesis routes of silver nanoparticles, in: Advances in Geotechnical and Transportation Engineering, Springer, 2020.
[33] L. Pourzahedi, M.J. Eckelman, Comparative life cycle assessment of silver nanoparticle synthesis routes, Environ. Sci. Nano 2 (2015) 361–369.
[34] S. Temizel-Sekeryan, A.L. Hicks, Global environmental impacts of silver nanoparticle production methods supported by life cycle assessment, Resour. Conserv. Recycl. 156 (2020), 104676.
[35] W. Wu, K. Bhattacharyya, K. Gray, E. Weitz, Photoinduced reactions of surface-bound species on titania nanotubes and platinized titania nanotubes: an in situ FTIR study, J. Phys. Chem. C 117 (2013) 20643–20655, https://doi.org/10.1021/jp405902a.

[36] M. Kotesh Kumar, K. Bhavani, G. Naresh, B. Srinivas, A. Venugopal, Plasmonic resonance nature of Ag-Cu/TiO2 photocatalyst under solar and artificial light: synthesis, characterization and evaluation of H2O splitting activity, Appl. Catal. B Environ. 199 (2016) 282–291, https://doi.org/10.1016/j.apcatb.2016.06.050.
[37] T. Wang, L. Chen, C. Chen, M. Huang, Y. Huang, S. Liu, et al., Engineering catalytic interfaces in Cu δ+/CeO_2-TiO_2 photocatalysts for synergistically boosting CO2 reduction to ethylene, ACS Nano 16 (2022) 2306–2318, https://doi.org/10.1021/acsnano.1c08505.
[38] L. Hurtado, R. Romero, A. Mendoza, S. Brewer, K. Donkor, R.M. Gómez-Espinosa, et al., Paracetamol mineralization by photo Fenton process catalyzed by a Cu/Fe-PILC under circumneutral pH conditions, J. Photochem. Photobiol. A Chem. (2019), https://doi.org/10.1016/j.jphotochem.2019.01.012.
[39] O. Avilés-García, J. Espino-Valencia, A. Mendoza-Zepeda, K. Donkor, S. Brewer, R. Romero, et al., Removal of metoprolol by means of photo-oxidation processes, Catal. Today (2021), https://doi.org/10.1016/j.cattod.2021.06.014.
[40] J. Jiao, Y. Wei, Y. Zhao, Z. Zhao, A. Duan, J. Liu, et al., AuPd/3DOM-TiO2 catalysts for photocatalytic reduction of CO2: high efficient separation of photogenerated charge carriers, Appl. Catal. B Environ. 209 (2017) 228–239, https://doi.org/10.1016/j.apcatb.2017.02.076.
[41] Y. Wei, J. Jiao, Z. Zhao, J. Liu, J. Li, G. Jiang, et al., Fabrication of inverse opal TiO2-supported Au@CdS core-shell nanoparticles for efficient photocatalytic CO2 conversion, Appl. Catal. B Environ. 179 (2015) 422–432, https://doi.org/10.1016/j.apcatb.2015.05.041.
[42] S. Zhu, W. Liao, M. Zhang, S. Liang, Design of spatially separated au and CoO dual cocatalysts on hollow TiO2 for enhanced photocatalytic activity towards the reduction of CO2 to CH4, Chem. Eng. J. 361 (2019) 461–469, https://doi.org/10.1016/j.cej.2018.12.095.
[43] A. Ziarati, A. Badiei, R. Luque, M. Dadras, T. Burgi, Visible light CO2 reduction to CH4 using hierarchical yolk@shell TiO2-xHx modified with plasmonic Au-Pd nanoparticles, ACS Sustain. Chem. Eng. 8 (2020) 3689–3696, https://doi.org/10.1021/acssuschemeng.9b06751.
[44] A. Pougin, G. Dodekatos, M. Dilla, H. Tüysüz, J. Strunk, Au@TiO2 core–shell composites for the photocatalytic reduction of CO2, Chem. Eur. J. 24 (2018) 12416–12425, https://doi.org/10.1002/chem.201801796.
[45] L. Collado, A. Reynal, J.M. Coronado, D.P. Serrano, J.R. Durrant, V.A. De la Peña O'Shea, Effect of Au surface plasmon nanoparticles on the selective CO2 photoreduction to CH4, Appl. Catal. B Environ. 178 (2015) 177–185, https://doi.org/10.1016/j.apcatb.2014.09.032.
[46] S. Cai, J. Chen, Q. Li, H. Jia, Enhanced photocatalytic CO2 reduction with photothermal effect by cooperative effect of oxygen vacancy and Au cocatalyst, ACS Appl. Mater. Interfaces 13 (2021) 14221–14229, https://doi.org/10.1021/acsami.0c23036.
[47] X. Wang, X. Xuan, Y. Wang, X. Li, H. Huang, X. Zhang, et al., Nano-au-modified TiO2 grown on dendritic porous silica particles for enhanced CO2 photoreduction, Microporous Mesoporous Mater. (2021) 310, https://doi.org/10.1016/j.micromeso.2020.110635.
[48] S. Bera, J.E. Lee, S.B. Rawal, W.I. Lee, Size-dependent plasmonic effects of Au and Au@SiO2 nanoparticles in photocatalytic CO2 conversion reaction of Pt/TiO2, Appl. Catal. B Environ. 199 (2016) 55–63, https://doi.org/10.1016/j.apcatb.2016.06.025.
[49] J. Bian, Y. Qu, X. Zhang, N. Sun, D. Tang, L. Jing, Dimension-matched plasmonic Au/TiO2/BiVO4 nanocomposites as efficient wide-visible-light photocatalysts to convert CO2 and mechanistic insights, J. Mater. Chem. A 6 (2018) 11838–11845, https://doi.org/10.1039/c8ta02889c.

[50] K. Khaletskaya, A. Pougin, R. Medishetty, C. Rösler, C. Wiktor, J. Strunk, et al., Fabrication of gold/titania photocatalyst for CO2 reduction based on pyrolytic conversion of the metal-organic framework NH2-MIL-125(Ti) loaded with gold nanoparticles, Chem. Mater. 27 (2015) 7248–7257, https://doi.org/10.1021/acs.chemmater.5b03017.
[51] I.H. Tseng, J.C.S. Wu, H.Y. Chou, Effects of sol-gel procedures on the photocatalysis of Cu/TiO2 in CO2 photoreduction, J. Catal. 221 (2004) 432–440, https://doi.org/10.1016/j.jcat.2003.09.002.
[52] S. Kreft, R. Schoch, J. Schneidewind, J. Rabeah, E.V. Kondratenko, V.A. Kondratenko, et al., Improving selectivity and activity of CO2 reduction photocatalysts with oxygen, Chem 5 (2019) 1818–1833, https://doi.org/10.1016/j.chempr.2019.04.006.
[53] S.N. Habisreutinger, L. Schmidt-Mende, J.K. Stolarczyk, Photocatalytic reduction of CO2 on TiO2 and other semiconductors, Angew. Chem. Int. Ed. 52 (2013) 7372–7408, https://doi.org/10.1002/anie.201207199.
[54] I. Bönicke, W. Kirstein, S. Spinzig, F. Thieme, CO adsorption studies on a stepped Cu(111) surface, Surf. Sci. 313 (1994) 231–238, https://doi.org/10.1016/0039-6028(94)90044-2.
[55] J.M. Gottfried, K.J. Schmidt, S.L.M. Schroeder, K. Christmann, Adsorption of carbon monoxide on Au(1 1 0)-(1 × 2), Surf. Sci. 536 (2003) 206–224, https://doi.org/10.1016/S0039-6028(03)00595-8.
[56] W. Li, A. Wang, X. Liu, T. Zhang, Silica-supported Au-Cu alloy nanoparticles as an efficient catalyst for selective oxidation of alcohols, Appl. Catal. A Gen. 433–434 (2012) 146–151, https://doi.org/10.1016/j.apcata.2012.05.014.
[57] M. Haruta, Size-and support-dependency in the catalysis of gold, Catal. Today 36 (1) (1997) 153–166.
[58] S.A. Gama-Lara, R.A. Morales-Luckie, L. Argueta-Figueroa, J.P. Hinestroza, I. García-Orozco, R. Natividad, Synthesis, characterization, and catalytic activity of platinum nanoparticles on bovine-bone powder: a novel support, J. Nanomater. 2018 (2018), https://doi.org/10.1155/2018/6482186.
[59] M. Compagnoni, A. Villa, E. Bahdori, D.J. Morgan, L. Prati, N. Dimitratos, et al., Surface probing by spectroscopy on titania-supported gold nanoparticles for a photoreductive application, Catalysts 8 (2018), https://doi.org/10.3390/catal8120623.
[60] K. Ji, H. Dai, J. Deng, H. Zang, H. Arandiyan, S. Xie, et al., 3DOM BiVO4 supported silver bromide and noble metals: high-performance photocatalysts for the visible-light-driven degradation of 4-chlorophenol, Appl. Catal. B Environ. 168–169 (2015) 274–282, https://doi.org/10.1016/j.apcatb.2014.12.045.
[61] T. Kamegawa, N. Suzuki, H. Yamashita, Design of macroporous TiO2 thin film photocatalysts with enhanced photofunctional properties, Energy Environ. Sci. 4 (2011) 1411–1416, https://doi.org/10.1039/C0EE00389A.
[62] J.C. Hemminger, R. Carr, G.A. Somorjai, The photoassisted reaction of gaseous water and carbon dioxide adsorbed on the $SrTiO_3$ (111) crystal face to form methane, Chem. Phys. Lett. 57 (1) (1978) 100–104.